Driven quantum spin chain in the presence of noise: Anti-Kibble-Zurek behavior

Manvendra Singh and Suhas Gangadharaiah
Department of Physics, Indian Institute of Science Education and Research, Bhopal 462066, India

(Received 10 March 2021; accepted 17 August 2021; published 31 August 2021)

We study defect generation in a quantum XY-spin chain arising due to the linear drive of the many-body Hamiltonian in the presence of a time-dependent fast Gaussian noise. The main objective of this work is to quantify analytically the effects of noise on the defect density production. In the absence of noise, it is well known that in the slow sweep regime, the defect density follows the Kibble-Zurek (KZ) scaling behavior with respect to the sweep speed. We consider time-dependent fast Gaussian noise in the anisotropy of the spin-coupling term [$\gamma_0 = (J_1 - J_2)/(J_1 + J_2)$] and show via analytical calculations that the defect density exhibits anti-Kibble-Zurek (AKZ) scaling behavior in the slow sweep regime. In the limit of large chain length and long time, we calculate the entropy and magnetization density of the final decohered state and show that their scaling behavior is consistent with the AKZ picture in the slow sweep regime. We have also numerically calculated the sublattice spin correlators for finite separation by evaluating the Toeplitz determinants and find results consistent with the KZ picture in the absence of noise, while in the presence of noise and slow sweep speeds the correlators exhibit the AKZ behavior. Furthermore, by considering the large n-separation asymptotes of the Toeplitz determinants, we further quantify the effect of the noise on the spin-spin correlators in the final decohered state. We show that while the correlation length of the sublattice correlator scales according to the AKZ behavior, we obtain different scaling for the magnetization correlators.

DOI: 10.1103/PhysRevB.104.064313

I. INTRODUCTION

A quantum system driven at zero temperature by some system dependent parameter through a quantum critical point (QCP) is subjected to quantum phase transition (QPT) in which the ground state of the system is fundamentally altered with completely different physical properties across the phase transition point. One of the main points of interest is to quantify the generation of excitations or the defect density generation due to the quench through the critical point. Defects are inevitable in a drive through the critical point due to the vanishing energy gap at the critical point where the adiabaticity criterion breaks down and nonadiabatic effects become important. In this regard, the Kibble-Zurek mechanism (KZM), a theory originally proposed to quantify the topological defect production in a cosmological phase transition has been successfully applied in quantifying the defect production in idealized condensed matter systems undergoing QPT [1–12]. The theory predicts that the defect density scales as $n \propto \tau_Q^{-\beta}$, where τ_Q is the quench time and the universal exponent $\beta > 0$ is determined by the critical exponents and the dimension of the system. Recent experimental studies supporting KZM have been reported in well controlled systems involving trapped ions, Bose-Einstein condensates, and Rydberg simulator [13–15].

While the study of quantum systems exhibiting KZ behavior remains an area of active interest, scenarios which result in deviations from this universal behavior have also come under increased scrutiny. Recent studies of drive protocols in quantum systems that are coupled to external environment, disorder, or are in the presence of noise indicate that the defect density generated exhibit fundamentally different dynamical behavior than the one predicted by the KZ theory [16–33]. The focus of our attention has been to understand analytically the experimental and numerical studies wherein, unlike the KZ behavior, slower drives beyond a certain optimal quench rate/speed create more defects [34–40]. This scaling has been termed as the anti-Kibble-Zurek (AKZ) behavior. In all of them, the AKZ scaling behavior manifested itself in the presence of the noisy control field driving the system through the critical points. In this work, we consider a time dependent quantum XY-spin chain which is driven by a transverse magnetic field with an anisotropy term that contains a fluctuating Gaussian noise term. In the limit of fast noise, we perform exact analytical calculations and derive the universal AKZ scaling behavior of the defect density with respect to the quench rate.

Apart from the study of the defect generation, the consequence of the KZ picture for the noiseless case to the entropy, magnetization, and the correlation functions has been considered before (for example in Refs. [28,41–45]). The entropy of the final state shows information loss due to decoherence in passing through the critical points, i.e., a finite nonzero entropy density at the end of the protocol is a sign of mixed state due to the defect generation. The presence of defects reduces the magnetization density. In addition, increase in defects results in reduced size of the ordered domains. Slower sweep speed results in reduced defect production; this consequently implies reduced entropy density, increased magnetization density, and enhanced correlation length at the

end of the drive protocol. In this work, we quantify the effect of noisy drive through the QCPs on the above mentioned physical quantities and show that they exhibit signatures of the AKZ behavior in the slow sweep regime. For quench times greater than the optimal quench time, the enhanced defect generation results in increased entropy density of the final decohered state, meanwhile, the magnetization density is suppressed. By considering the large n-separation asymptotes of the Toeplitz determinants, we calculate the correlation lengths of the sublattice correlators and show that the correlation length of the spin correlators decreases for slow sweep rates consistent with the AKZ scaling picture. However, the correlation length of the (connected) magnetization correlator in the large n-separation limit continues to follow the KZ picture.

The organization of the paper is as follows. In Sec. II we discuss the model Hamiltonian and dynamics of the XY-spin chain with transverse magnetic field (varying linearly with time) in the z direction in the absence of noise. In Sec. III we consider transverse protocol in the presence of fast Gaussian noise and obtain analytically the AKZ scaling behavior of the defect density in the slow drive regime. We also derive an expression for the optimal quench time with which the system must be driven so as to minimize the defect production at the end of the drive protocol. In Sec. IV we discuss the decoherence of the local observables due to the drive through the QCPs in the presence of Gaussian noise and in addition the expectation values of a fermionic two-point correlator in the final decohered state has been obtained. In Sec. V we derive the analytical expression for the entropy density for the final decohered state and show that the results are consistent with the AKZ scenario. Finally, in Sec. VI we discuss in detail the analytical results for the spin correlators and the magnetization density at the end of the noisy drive protocol. We have summarized our results in Sec. VII.

II. THE MODEL HAMILTONIAN

We consider the quantum XY-spin model driven by the transverse external field $h(t)$,

$$H(t) = -\sum_{n=1}^{N}\left[J_1\sigma_n^1\sigma_{n+1}^1 + J_2\sigma_n^2\sigma_{n+1}^2 + h(t)\sigma_n^3\right], \quad (1)$$

where J_1 and J_2 are, respectively, the spin-spin couplings along the x- and y-spin directions. Introducing the coefficients $J = J_1 + J_2$ and anisotropy, $\gamma_0 = (J_1 - J_2)/J$, allows us to re-express the Hamiltonian as

$$H(t) = -\frac{J}{2}\sum_{n=1}^{N}\left[(1+\gamma_0)\sigma_n^1\sigma_{n+1}^1 + (1-\gamma_0)\sigma_n^2\sigma_{n+1}^2\right] - h(t)\sum_{n=1}^{N}\sigma_n^3. \quad (2)$$

The $\gamma_0 = 0$ limit represents the isotropic XY-spin chain, while $\gamma_0 = \pm 1$ limits correspond to the quantum Ising chain case. We consider time dependence in the anisotropy by including Gaussian correlated noise $\eta(t)$, i.e., $\gamma_0 \to \gamma(t) = \gamma_0 + \eta(t)$. The Gaussian noise $\eta(t)$ is characterized by

$$\overline{\eta(t)} = 0, \ \overline{\eta(t)\,\eta(t_1)} = \eta_0^2\, e^{-\Gamma|t-t_1|}, \quad (3)$$

where η_0 is the noise strength and Γ is the inverse time scale associated with the noise.

In the following, we will summarize the well studied transverse protocol [41,46,47]. In this protocol, the transverse external field $h(t)$ is tuned to drive the equilibrium system from $h \to -\infty$ at the start of the protocol to $h \to \infty$ at the end of the drive protocol. For a linear protocol,

$$h(t) = vt = Jt/\tau_Q,$$

where v is the sweep speed of the drive, $\tau_Q = J/v$ is the 'quench time,' and the time t runs from $-\infty$ to ∞. The system starts out in the paramagnetic (PM) ground state (GS), $|\downarrow\downarrow\downarrow \ldots \downarrow\rangle$ with all the spins along the negative z axis. As t is increased the system goes through the QCPs at $h(t) = \pm J$. The quantum phase transition involves change in the nature of GS from PM to ferromagnetic (FM) at $h = -J$ and from FM to PM at $h = J$. The final state that emerges is not the perfect GS of the Hamiltonian, $|\uparrow\uparrow\uparrow \ldots \uparrow\rangle$, but instead is formed out of the quantum superposition of the states of the type $|..\uparrow\uparrow\downarrow\uparrow\uparrow\uparrow\uparrow\downarrow\uparrow\uparrow ..\rangle$. The reason for such a final state is the inevitable violation of the adiabaticity criteria. This criteria is obtained by comparing two time scales, the relaxation time scale, which is proportional to the inverse of minimum gap of the system, and a time scale for driving the system, τ_Q. For a perfectly adiabatic dynamics, 'relaxation time $\ll \tau_Q$.' But in the $N \to \infty$ limit, the energy gap vanishes at the QCPs $[h(t) = \pm J]$. Therefore the dynamics becomes nonadiabatic in close proximity to the QCPs, leading to a final state which is formed out of the quantum superposition of the states having kinks/domain walls.

It turns out that rate of production of these topological defects can be quantified with the help of KZ scaling theory. Qualitatively one can understand the theory as follows [48]. The energy gap around the QCP depends on the driving field, $\Delta(h) \sim |h - h_c|^{\nu z_d} \sim |vt|^{\nu z_d}$ (assuming the gap varies linearly with time) with ν being the correlation length exponent and z_d the dynamical exponent. The correlation length diverges near the QCP as $\xi \sim |h - h_c|^{-\nu}$, whereas the excitation energy, $E(k, h = h_c) \sim |k - k_c|^{z_d}$, characterized by the dynamical exponent z_d, vanishes near the critical mode k_c. The region where the adiabaticity breaks down called the nonadiabatic/impulse region (near the QCP) can be estimated by comparing the rate of change of the driving parameter/energy gap with the energy which is proportional to the square of the energy, i.e., $d\Delta/dt \approx \Delta^2$. One finds that the energy scale at which the adiabaticity breaks down is given by $\Delta^* \sim |v|^{\nu z_d/(\nu z_d+1)}$. Corresponding to this energy scale a length scale $\xi^* \sim |v|^{-\nu/(z_d\nu+1)}$ can be associated beyond which the fluctuations of the order parameter cannot follow the adiabatic dynamics resulting in the creation of defects/excitations.

$$n \sim |\xi^*|^{-d} \sim |v|^{\nu d/(\nu z_d+1)} \propto |\tau_Q|^{-\nu d/(\nu z_d+1)}, \quad (4)$$

where d is the dimension of the system. For a 1D XY-spin chain undergoing a transverse protocol (linearly with time) and $\nu = z_d = 1$, the KZ scaling theory predicts the defect density to scale as $n \sim \sqrt{v} \sim 1/\sqrt{\tau_Q}$.

These predictions were confirmed by the exact solution of the defect density generation in a linearly driven XY-spin chain Hamiltonian by mapping it to a set of independent

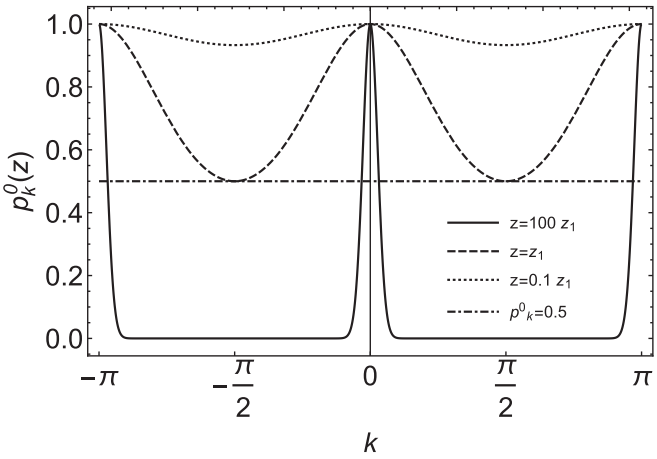

FIG. 1. p_k^0 vs k in the absence of noise. In the large z or the small sweep speed limit, most of the contribution to the defect generation comes from the regions near the critical points $k = 0, \pm\pi$. It is to be noted that $z_1 = \log 2/2\pi$ is a special value of z, where $p_k^0 = 1/2$ at $k = \pm\pi/2$.

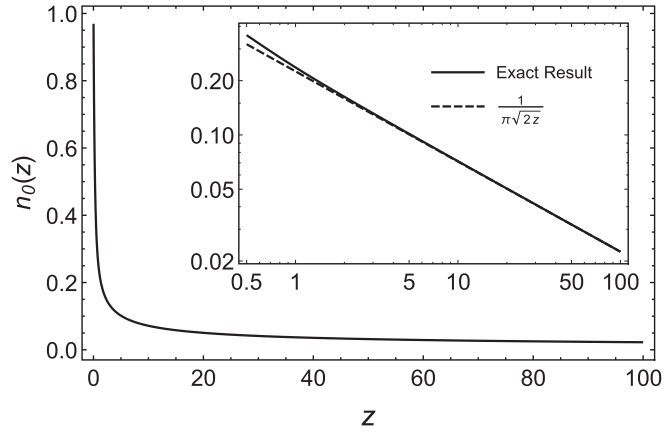

FIG. 2. $n_0(z)$ vs z in the absence of noise. Plotted is the exact result for the defect density. The log-log plot in the inset shows the exact result and the approximate result (scaling behavior as predicted by the KZ scenario) coincide for large z values.

two-level Landau-Zener (LZ) problems. The first step involves the use of Jordan-Wigner (JW) transformation, $\sigma_n^{\pm} = (e^{\pm i\pi \sum_{l=1}^{n-1} c_l^{\dagger} c_l}) c_n$ and $\sigma_l^z = 2c_l^{\dagger} c_l - 1$ (with $\sigma_l^{\pm} = \sigma^x \pm i\sigma^y$), to map the spin-1/2 Hamiltonian to the spinless free fermion Hamiltonian

$$H(t) = -J \sum_{n=1}^{N} [(c_n^{\dagger} c_{n+1} + \gamma_0 c_{n+1} c_n + \text{H.c.}) - h(t)(2c_n^{\dagger} c_n - 1)]. \quad (5)$$

Restricting to the even parity subspace with $c_{N+1} = -c_1$ and using the Fourier transformation, $c_n = \frac{e^{-i\pi/4}}{\sqrt{N}} \sum_k c_k e^{ikn}$ yields

$$H(t) = \sum_k \left[(h(t) + J\cos k) c_k^{\dagger} c_k + \frac{\Delta_k}{2} c_{-k} c_k \right] + \text{H.c.}, \quad (6)$$

where $\Delta_k = 2J\gamma_0 \sin(k)$. The above Hamiltonian can be written as a sum of independent terms, $H(t) = \sum_{k>0} H_k(t)$, where for each value of k, $H_k(t)$ acts on the four-dimensional Hilbert space spanned by the basis vectors: $|0\rangle$, $|k\rangle = c_k^{\dagger}|0\rangle$, $|-k\rangle = c_{-k}^{\dagger}|0\rangle$ and $|k,-k\rangle = c_k^{\dagger} c_{-k}^{\dagger}|0\rangle$. We note that the Hamiltonian with or without the noise term proportional to $\eta(t)$ leaves the parity unchanged. Although the one-particle states $|k\rangle$ and $|-k\rangle$ evolve in time with a global phase factor only, the states $|0\rangle$ and $|k,-k\rangle$ couple to each other and exhibit LZ dynamics. The projected Hamiltonian in the subspace of $|0\rangle$ and $|k,-k\rangle$ has the structure of LZ type Hamiltonian and is given by

$$\mathcal{H}_k(t) = 2 \begin{bmatrix} h(t) + J\cos(k) & \Delta_k/2 \\ \Delta_k/2 & -h(t) - J\cos(k) \end{bmatrix}, \quad (7)$$

where we note that the off-diagonal term is k-dependent. Applying the LZ transition theory yields the k-dependent transition/excitation probability (in the large time limit),

$$p_k^0(z) = e^{-2\pi z \sin^2 k}, \quad (8)$$

where z is the dimensionless quench parameter given by $z = J^2\gamma_0^2/v = J\gamma_0^2\tau_Q$ (see Fig. 1).

The total defect density is thus given by $n_0(z) = \sum_{k>0} p_k^0(z)/N$. In the $N \to \infty$ limit, the summation over the k modes is replaced by integration. Performing the integration one obtains the exact result for the total defect density n_0 in the absence of noise,

$$n_0(z) = \frac{1}{\pi} \int_0^{\pi} dk\, e^{-2\pi z \sin^2 k} = e^{-\pi z} I_0[\pi z], \quad (9)$$

where $I_0(\pi z)$ is the modified Bessel function of the first kind. The limit of large z (or the small sweep speed regime) reveals that the defect density scales as $n_0 \sim 1/\sqrt{z}$, which indeed matches with the prediction of the KZ scaling behavior (see Fig. 2).

Interestingly, recent numerical studies have shown that the defect density production exhibits completely different scaling when in addition to the usual linear protocol a small Gaussian noise is present in the control field [36,37]. In particular, the defect density scales as

$$n \approx c\, \tau_Q^{-1/2} + d\, \eta^2\, \tau_Q, \quad (10)$$

where c and d are system dependent parameters. The first term in the above equation Eq. (10) accounts for the usual KZ scaling behavior. The second term is proportional to the square of noise amplitude and represents increased defect-density production with the increase of τ_Q (or is inversely proportional to the sweep speed). This is converse to that of the KZ scaling and is termed the AKZ scaling behavior.

In the next section we will consider linear protocol with transverse noise and obtain analytical results for the defect density. We will show that for large-z values AKZ scaling behavior dominates. In the subsequent sections, we will calculate the entropy and correlation functions of a driven quantum XY-spin chain in the presence of noise.

III. EFFECT OF NOISE ON THE DEFECT GENERATION

The time dynamics of states spanned by $|0\rangle$ and $|k,-k\rangle$ is governed by the Hamiltonian $\mathcal{H}_k^\eta(t)$,

$$\mathcal{H}_k^\eta(t) = 2\begin{bmatrix} h(t)+J\cos(k) & J\,\gamma_0\sin(k) \\ J\,\gamma_0\sin(k) & -h(t)-J\cos(k)\end{bmatrix} + 2\,\eta(t)\begin{bmatrix} 0 & J\,\sin(k) \\ J\,\sin(k) & 0\end{bmatrix}, \tag{11}$$

where the first term in the above Hamiltonian is the usual deterministic part. The second term couples the homogeneous time-dependent Gaussian noise $\eta(t)$ to each of the k mode within the restricted subspace. In this subspace, a general state at any given time t for a single realization of the noise $\eta(t)$ can be written as $|\Psi_k^\eta(t)\rangle = u_k^\eta(t)|0\rangle + v_k^\eta(t)|k,-k\rangle$, where $u_k^\eta(t)$ and $v_k^\eta(t)$ are the time-dependent amplitudes. The system starts out in the perfect PM state defined by the initial conditions $u_k^\eta(-\infty)=1$ and $v_k^\eta(-\infty)=0$. The time evolution of the general state $|\Psi_k^\eta(t)\rangle$ for a single noise realization is governed by the stochastic Schrödinger equation,

$$i\frac{d}{dt}\big|\Psi_k^\eta(t)\big\rangle = \mathcal{H}_k^\eta(t)\big|\Psi_k^\eta(t)\big\rangle, \tag{12}$$

where the solution has to be averaged over all possible realizations (ensemble averaging due to the noise) of the two-level system corresponding to each k mode [49–51].

The projected Hamiltonian Eq. (11) is equivalent to the noisy LZ problem with the noise present only in the transverse part of the Hamiltonian. We consider the density matrix, $\hat{\rho}_k^\eta(t) = |\Psi_k^\eta(t)\rangle\langle\Psi_k^\eta(t)|$, and set up the time evolution equation for the population inversion ρ_k^η (difference between the unexcited and the excited density for a given mode k):

$$\frac{d}{d\tau}\rho_k^\eta(\tau) = -\frac{1}{2}\int_{-\infty}^{\tau} d\,\tau_1 e^{i\int_{\tau_1}^{\tau} d\tau_2\,(v_{\rm LZ}\tau_2)/2}\,\rho_k^\eta(\tau_1) - \frac{1}{2\,\gamma_0^2}\int_{-\infty}^{\tau} d\,\tau_1 e^{i\int_{\tau_1}^{\tau} d\tau_2\,(v_{\rm LZ}\tau_2)/2} \times \eta(\tau)\eta(\tau_1)\,\rho_k^\eta(\tau_1) + \text{H.c.}, \tag{13}$$

where $\tau = 2\Delta_k(t+\cos k/v)$, and $v_{\rm LZ} = v/\Delta_k^2$. Taking the noise average one obtains

$$\frac{d}{d\tau}\rho_k(\tau) = -\int_{-\infty}^{\tau} d\,\tau_1\cos\left[\frac{v_{\rm LZ}}{4}\left(\tau^2-\tau_1^2\right)\right]\rho_k(\tau_1) - \frac{1}{\gamma_0^2}\int_{-\infty}^{\tau} d\,\tau_1\cos\left[\frac{v_{\rm LZ}}{4}\left(\tau^2-\tau_1^2\right)\right] \times \overline{\eta(\tau)\eta(\tau_1)}\,\rho_k(\tau_1), \tag{14}$$

where $\rho_k(\tau_1)$ is obtained by performing noise average over $\overline{\rho_k^\eta(\tau_1)}$. The fast noise criteria ($\Gamma^{-1} \ll \tau_Q$) allows us to decouple $\overline{\eta(\tau)\eta(\tau_1)\rho_k^\eta(\tau_1)}$ into a separate product of the noise terms and the density matrix term, $\overline{\eta(\tau)\eta(\tau_1)}\,\rho_k(\tau_1)$ [50]. The solution of the reduced master equation in the $t\to\infty$ limit is obtained by following the approach of Ref. [50] and is given by $\rho_k = e^{-2\pi\,\eta_0^2/(2\,v_{\rm LZ}\,\gamma_0^2)}(2\,e^{-\pi/(2\,v_{\rm LZ})}-1)$. The noise averaged excitation probability thus obtained in the fast noise regime is

$$p_k(z) = \tfrac{1}{2}\left[1+e^{-4\pi z\,\eta_1^2\sin^2 k}\,(2\,e^{-2\pi z\sin^2 k}-1)\right], \tag{15}$$

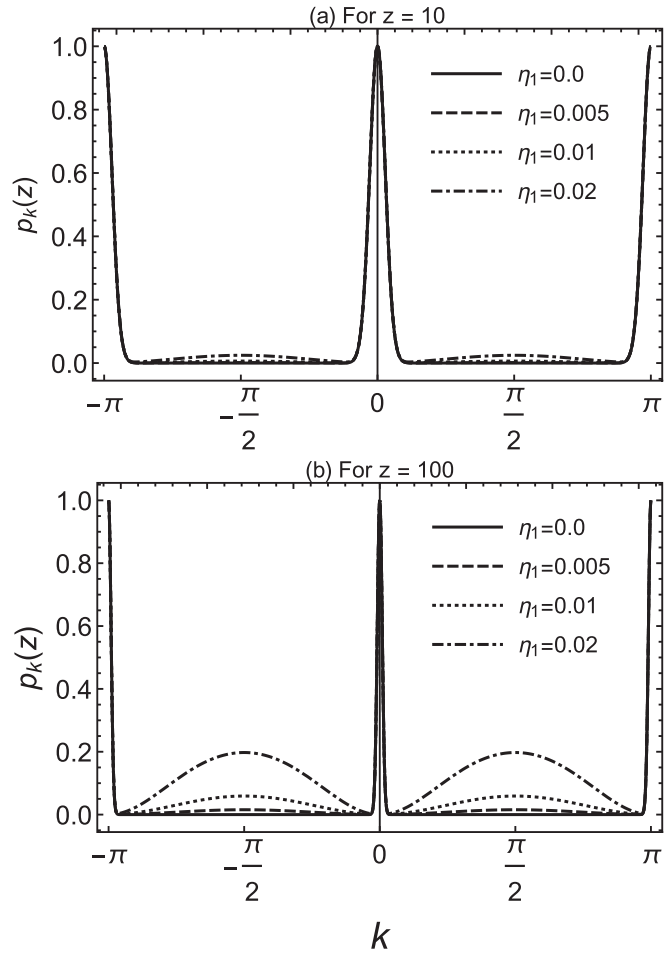

FIG. 3. p_k vs k in the presence of the fast noise: Interestingly, in the large-z regime ($z \gg z_1$) or slower sweeps the fast noise begins to affect the system. New critical region (where the excitation probability becomes nonzero) opens up symmetrically around $k = \pm\pi/2$ resulting in more defect generation.

where $\eta_1 = \eta_0/\gamma_0$. It is interesting to note that the excitation probability [Eq. (15)], which is nonzero around the $k = 0, \pm\pi$ points in the absence of noise, also opens up around $k = \pm\pi/2$ regions in the presence of noise and in particular for the large z limit or the small sweep speed scenario, which is the result of dephasing due to the presence of the fast noise which is one of the main reasons for more defect generation for slower sweeps (see Fig. 3). Recently, similar results have been reported in Ref. [52] for the noisy drive protocols in a trapped ion experiment. It is worth noting that the fast sweep regime ($z \ll z_1$) is unaffected by the fast noise.

We next evaluate the defect density by integrating $n(z) = \int_0^\pi dk\,p_k/\pi$ and obtain

$$n(z) = \tfrac{1}{2} + e^{-\pi\,(z+\bar{z})}\,I_0[\pi\,(z+\bar{z})] - \tfrac{1}{2}e^{-\pi\bar{z}}I_0[\pi\bar{z}], \tag{16}$$

where $\bar{z} = 2z\eta_1^2$. The focus of our interest is in the scaling of the defect density in the slow sweep ($z \gg 1$) and weak noise ($\eta_1 \ll 1$) regimes, such that $\pi\bar{z} < 1$. In this limit, the defect density is approximated as

$$n(z) \approx \frac{1}{\pi\sqrt{2z}} + \pi\eta_1^2 z, \tag{17}$$

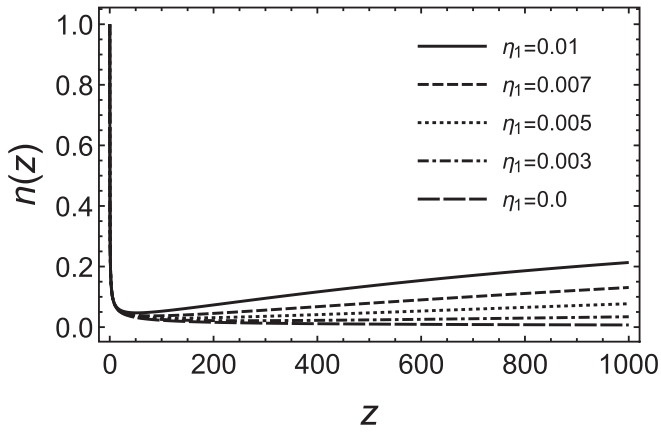

FIG. 4. Effect of the fast noise on the defect density: The defect density has been plotted with respect to z for different noise strength, which is consistent with the AKZ picture for large-z regime i.e., enhanced defect generation for sweep rates slower than the optimal quench rate.

which gives the AKZ scaling behavior (see Figs. 4 and 5). Therefore, it can be deduced that the defect density is minimized for a optimal z given by

$$z_{\rm O} \approx 2\sqrt{2}\,\pi^2 \eta_1^{-4/3} \propto \eta_1^{-4/3}, \tag{18}$$

and hence the optimal quench time scales as $\tau_{\rm O} \propto \eta_0^{-4/3}$ with respect to the noise strength. We note that the defect density in the slow sweep regime, given by Eq. (17), in its most general form can be written in terms of the equilibrium critical exponents as $n(\tau_Q) = c\tau_Q^{-\beta} + d\eta_0^2\tau_Q$, where $\beta = \nu d/(\nu z_d + 1)$ is the universal KZM exponent, while c and d as mentioned earlier are the system dependent parameters. The origin of the second term can be attributed to the presence of fast Gaussian noise in the limit of weak noise strength when expanded up to the second order in perturbative expansion. By minimizing the defect density, one obtains $\tau_{\rm O} \propto \eta_0^{-2/(\beta+1)}$, which implies universal power law scaling of the optimal quench time $\tau_{\rm O}$ ($\propto z_{\rm O}$) with the noise strength. For our case this results in Eq. (18). The power law universality of the optimal quench

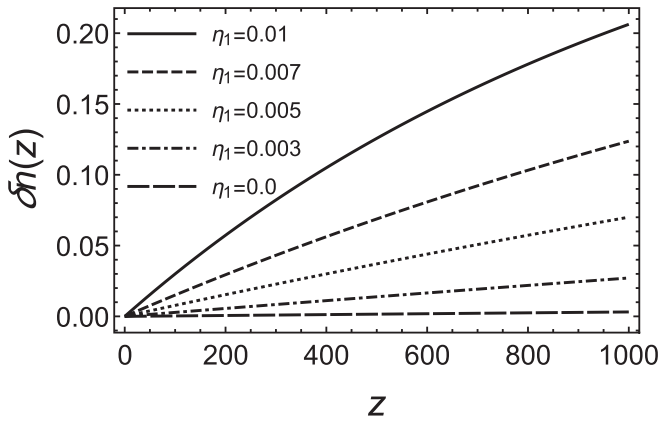

FIG. 5. Anti-Kibble-Zurek scaling behavior of the defect density: The difference, $\delta n = n(z) - n_0(z)$, scales linearly with z for weak noise strengths and $\pi\bar{z} < 1$.

time with the noise strength has also been shown in the numerical studies in Refs. [36,37] and in an experimental work in Ref. [52].

While the above results have been obtained in the thermodynamic limit, we will briefly discuss the regime for which the results continue to hold in the leading order for the finite-N scenario. The generation of nonzero defects in a quantum critical system in the presence of the external drive is due to the nonadiabatic effects around the critical points. The effect of finite size is reflected in the nonzero energy gap at the critical points. To ensure that the diabatic effects are observed, the quench rate should be fast enough such that the lowest modes, $k = \pm\pi/N$, get excited. This is ensured if $z < N^2/2\pi^3$ (i.e., $p_{\pi/N}$ is not exponentially suppressed) or in other words the constraint on the quench time for diabatic effects are $\tau_Q < N^2/2\pi^3 J\gamma_0^2$ (which is always satisfied in the thermodynamic limit). Moreover, taking into account the criterion considered for obtaining Eq. (17) puts the following constraint on the quench time $1/J\gamma_0^2 \ll \tau_Q < \min[1/2\pi J\eta_0^2,\ N^2/2\pi^3 J\gamma_0^2]$. In this regime, it is expected that the leading order results for the finite-N chain to match with those obtained from the thermodynamic limit case as given in Eq. (17).

IV. DECOHERENCE OF LOCAL OBSERVABLES

In both the noiseless and noisy drive protocols, the XY-spin chain (with N spins) is prepared in a PM state at the initial time $t_{\rm in} = -T$. This initial state is a pure state, i.e., the full system density matrix can be written as $\rho(t = -T) = |0_N\rangle\langle 0_N|$. Subsequently the system is driven by the transverse magnetic field $h(t) = Jt/\tau_Q$ through the quantum critical points ($h = \mp J$) up to the final time $t_f = T$. In the noiseless drive scenario the full density matrix of the evolved N-spin chain remains in the pure state due to the unitary time evolution. However, for large system size ($N \to \infty$) and in the long time limit, i.e., $T \to \infty$, the coherences of the density matrix develop highly fluctuating phases (dependent on k and T) which vanish when integrated over k for all local observables [41]. This decohered density matrix corresponds to the nonequilibrium steady state (NESS) which is fundamentally different from the decoherence process due to any external or internal noise [41]. In addition to the internal decoherence the dephasing is further enhanced by the noise in the drive protocol which results in the exponential suppression of the fluctuating coherences.

For k-values such that $\eta_0^2 J \ll \Delta_k$, the noise has negligible effect on the system. The crossover region is around $\eta_0^2 J \sim \Delta_k$ at which the noise begins to play a role in the dynamics of the system. In the limit $\eta_0^2 J \gg \Delta_k$, the fast noise effects the system the most specifically in the nonadiabatic regions (when the gap $\Delta_k \to 0$) around the quantum critical points ($k = 0, \pm\pi$), in addition new critical regions around $k = \pm\pi/2$ become important. Overall, nonadiabatic effects are enhanced due to the noise which gives incoherent contributions to the defect density leading to increased defect generation at the end of the protocol.

In the long time limit, the noise averaged off-diagonal terms of the density matrix (coherences), $\bar{\rho}_{12}^k$ and $\bar{\rho}_{21}^k$ vanish. Therefore the noise averaged decohered density matrix, $\bar{\rho}_D = \otimes_{k>0}\bar{\rho}_{D,k}$ (with $\bar{\rho}_{D,k}$ a diagonal 2×2 matrix in the subspace

$|0\rangle, |k, -k\rangle)$ in the limit $N \to \infty$ and $T \to \infty$, with respect to the final decohered state can be written as

$$\bar{\rho}_{D,k} = \begin{pmatrix} p_k & 0 \\ 0 & 1-p_k \end{pmatrix}. \tag{19}$$

We will use the above expression of the density matrix to calculate the noise averaged observables in the final decohered state.

Two-point correlator in the fermionic representation

Similar to Ref. [41], one can define a two-point correlator in terms of the fermionic operators as

$$d\,(x-x') = \langle c_x\, c^{\dagger}_{x'}\rangle = \frac{1}{2\pi}\int_{-\pi}^{\pi} dk\, e^{-ik\,(x-x')}\, p_k. \tag{20}$$

This correlator is nonzero for $x - x' = 2n$, where n is an integer. In the absence of noise the two-point correlator is

$$d_n(z) = \frac{1}{2\pi}\int_{-\pi}^{\pi} dk\, e^{-ikn}\, p_k^0 = e^{-\pi z}\, I_n(\pi z), \tag{21}$$

where $I_n(\pi z)$ is the modified Bessel function of the first kind. The large-n expansion of d_n at fixed z yields

$$d_n(z) \approx \frac{1}{2\pi}\int_{-\pi}^{\pi} dk\, e^{-\pi z k^2/2} e^{ink} = \frac{e^{-n^2/2\pi z}}{\sqrt{2\pi^2 z}}. \tag{22}$$

Thus consistent with the KZ picture the correlation length of the two-point correlator is proportional to $\sqrt{z}$ and the magnitude of the correlator is inversely proportional to $\sqrt{z}$.

A similar calculation for the two-point correlator in the presence of noise, p_k yields

$$\begin{aligned} d_n(z) &= \frac{1}{2\pi}\int_{-\pi}^{\pi} dk\, e^{-ikn}\, p_k \\ &= \frac{1}{2}\delta_{n,0} - \frac{1}{2}e^{-\pi\bar{z}} I_n[\pi\bar{z}] + e^{-\pi(z+\bar{z})}\, I_n[\pi(z+\bar{z})]. \end{aligned} \tag{23}$$

In the limit of $\eta_1 \ll 1$ and $\pi\bar{z} < 1$ and for large-n expansion $(n > \sqrt{4\pi z\eta_1^2 \ln 1/\eta_1})$ the above expression is approximated as

$$d_n(z) \approx \frac{1}{\sqrt{2\pi^2(z+\bar{z})}} e^{-n^2/[2\pi(z+\bar{z})]}. \tag{24}$$

Thus the correlation length in the presence of noise $l_n = \sqrt{\pi(z+\bar{z})}$ remains proportional to $\sqrt{z}$ and increases with the strength of the noise.

V. ENTROPY DENSITY IN THE FINAL DECOHERED STATE

The decohered state has a finite entropy density which is a clear indication that the final state is a mixed state. To quantify the amount of information lost in the decoherence process (at the end of the drive protocol) we calculate the Von-Neumann entropy ($S = -N \mathrm{tr}\, \rho_D \ln \rho_D$) in terms of the excitation probability as follows,

$$S = -\frac{N}{2\pi}\int_{-\pi}^{\pi} dk[p_k \ln p_k + (1-p_k)\ln(1-p_k)], \tag{25}$$

where p_k is given in Eq. (15). The above integration is performed by expanding both the log terms in terms of $e^{-4\pi z\eta_1^2 \sin^2 k}(2e^{-2\pi z \sin^2 k} - 1)$ and integrating each of the terms individually. The final result of the entropy density (S/N) can be expressed in the following series form,

$$S/N = \ln 2 - \sum_{m=1}^{\infty}\sum_{r=0}^{2m} \frac{2^{2m-r}(-1)^r \binom{2m}{r}}{2m\,(2m-1)} e^{-\pi z Y_m^r} I_0\left[\pi z Y_m^r\right], \tag{26}$$

where $Y_m^r = (2m - r + 4m\eta_1^2)$. In Fig. 6 we plot Eq. (26) for different noise strengths. One can observe from the figure that the finite entropy density depends on the sweep speed and also that for each noise strength there exists an optimal quench parameter ($\sim z_O$) either side of which the entropy density increases. In particular, for z greater than this parameter the entropy increases which is the signature of AKZ behavior of defect production. For $\eta_1 \neq 0$, the entropy density asymptotically approaches ln 2 for large-z value, i.e., a fully mixed state is formed or in other words, the system approaches an asymptotic infinite temperature steady state. However, for the fast sweep speeds ($z < z_1$), the driven system is not affected by the noise. In the intermediate region the system has some finite nonzero entropy density which signifies a partially mixed state.

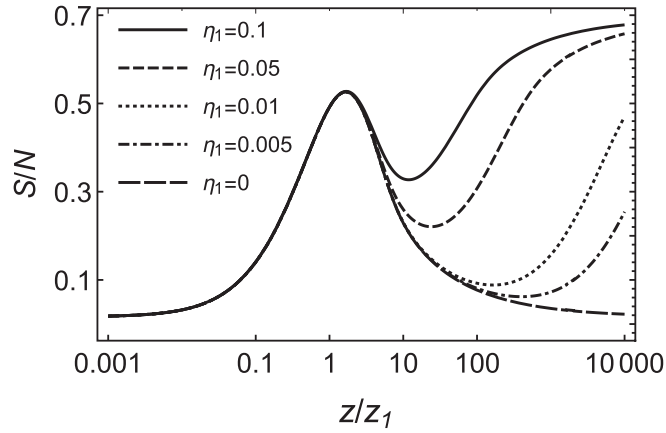

FIG. 6. Entropy density S/N vs z plotted for different noise strengths. The behavior of entropy density is consistent with the AKZ picture. The entropy density increases for quench time greater than the quench time $\sim\tau_O$ which is the signature of increased defect generation due to the fast noise in slower sweep regime. For very slow sweeps, the noise (even for $\eta_1 \ll 1$) can randomize the system to the maximally mixed state (i.e., $S/N \to \ln 2$). Apart from that, the entropy density maximizes (locally) at $z = z_1$ which is the signature of the crossover behavior of the spin correlation functions from monotonically decreasing behavior for $z < z_1$ to the oscillatory behavior for $z > z_1$ as discussed in Ref. [41].

VI. MAGNETIZATION AND SPIN-SPIN CORRELATIONS

The expectation value of the spin-spin correlators with respect to the decohered state is conveniently obtained in terms of the pair products of Majorana fermion operators. Consider the Majorana fermion operators [28,41,53,54]

$$A_x = c_x^{\dagger} + c_x, \quad B_x = c_x^{\dagger} - c_x. \tag{27}$$

The pair product of spins $\sigma_x^\alpha\,\sigma_{x+n}^\alpha$ and that of the Jordan-Wigner string variable $\tau_x\tau_{x+n}$ [with $\tau_x = \Pi_{x'<x}(-\sigma_{x'}^3)$] can be expressed as follows [41],

$$\sigma_x^1\,\sigma_{x+n}^1 = B_xA_{x+1}B_{x+1}....A_{x+n-1}B_{x+n-1}A_{x+n}, \tag{28}$$

$$\sigma_x^2\,\sigma_{x+n}^2 = A_xA_{x+1}B_{x+1}....A_{x+n-1}B_{x+n-1}B_{x+n}, \tag{29}$$

$$\tau_x\tau_{x+n} = A_xB_xA_{x+1}B_{x+1}....A_{x+n}B_{x+n}. \tag{30}$$

Due to the sublattice structure of the decohered matrix, i.e., decoupling of the decohered matrix, $\rho_D = \rho_E \otimes \rho_O$, with ρ_E and ρ_O acting correspondingly on the even and odd sublattice only, the expectation values of the full lattice spin correlators can be written as a product of sublattice correlators as follows [41],

$$\left\langle\sigma_x^\alpha\,\sigma_{x+2n}^\alpha\right\rangle = \left\langle\left\langle\sigma_x^\alpha\,\sigma_{x+n}^\alpha\right\rangle\right\rangle\langle\langle\tau_x\,\tau_{x+n}\rangle\rangle,\ \ \alpha = 1, 2. \tag{31}$$

$$\langle\tau_x\,\tau_{x+2n}\rangle = \langle\langle\tau_x\,\tau_{x+n}\rangle\rangle\,\langle\langle\tau_x\,\tau_{x+n}\rangle\rangle, \tag{32}$$

where $\langle ...\rangle$ and $\langle\langle ...\rangle\rangle$ represent the expectation values on the full lattice and the sublattice, respectively. The sublattice correlators are obtained using the Wick's theorem which requires one to evaluate correlators of the form $\langle B_xA_{x'}\rangle$, $\langle A_xB_{x'}\rangle$, $\langle A_xA_{x'}\rangle$, and $\langle B_xB_{x'}\rangle$. Out of these only the correlators of the type $\langle B_xA_{x'}\rangle$, $\langle A_xB_{x'}\rangle$ are needed to calculate the sublattice correlators which can be expressed in the form of the Toeplitz determinants.

The expectation value of the magnetization operator m_z, evaluated with respect to the final decohered state and in terms of the Majorana operators, is given by

$$m_z = \left\langle\sigma_x^3\right\rangle = \langle A_xB_x\rangle, \tag{33}$$

and the expectation value of the magnetization correlator is given by

$$\left\langle\sigma_x^3\,\sigma_{x'}^3\right\rangle = \langle A_xB_xA_{x'}B_{x'}\rangle. \tag{34}$$

We first evaluate the magnetization and magnetization correlators following which we discuss $\sigma_x^{1,2}$ spin-spin correlators.

A. Magnetization density and magnetization correlation

The average magnetization density $\langle\sigma_x^3\rangle$ at the end of the quench protocol is given by

$$m_z = \langle A_x\,B_x\rangle = 1 - 2n(z), \tag{35}$$

where $n(z)$ is the noise dependent defect density [Eq. (16)] and in terms of which

$$m_z = e^{-\pi\bar{z}}I_0[\pi\bar{z}] - 2\,e^{-\pi(z+\bar{z})}\,I_0[\pi(z+\bar{z})]. \tag{36}$$

Thus the large-z limit of the magnetization density given by

$$m_z - 1 \approx -\frac{1}{\sqrt{2}\,\pi\,\sqrt{z}} - \pi z\eta_1^2 \tag{37}$$

is consistent with the AKZ picture or in other words, it decreases after the optimal quench time, Eq. (18), when the defect production starts to increase due to the noise (see Fig. 7). In contrast, for the noiseless drive case (i.e., for $\eta_1 = 0$ in Fig. 7), the magnetization density asymptotically approaches unity for $z \gg 1$.

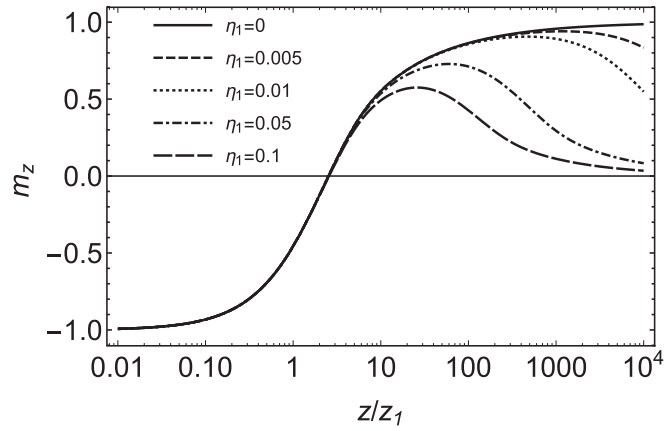

FIG. 7. Magnetization density as a function of z reduces after the optimal quench time in agreement with the AKZ picture. For the very large-z case, the noise randomizes the system completely resulting in a zero magnetization density.

Consider next the magnetization correlator in the z direction, $\langle\sigma_x^3\,\sigma_{x+2n}^3\rangle$, given by

$$\left\langle\sigma_x^3\,\sigma_{x+2n}^3\right\rangle = \left\langle\sigma_x^3\right\rangle^2 - \left(2\int_{-\pi}^{\pi}\frac{dk}{2\pi}\,e^{-ikn}p_k\right)^2. \tag{38}$$

The connected correlator $C_n(z)$ is obtained by subtracting the position independent part, $\langle\sigma_x^3\rangle^2$ from $\langle\sigma_x^3\,\sigma_{x+2n}^3\rangle$ and is given by $C_n(z) = -4d_n^2(z)$, where $d_n(z)$ is given by Eq. (23). Therefore, the magnetization correlation for large n retains the KZ scaling relation with the correlation length given by

$$l_{\text{noisy}} = \sqrt{\pi(z+\bar{z})/2}, \tag{39}$$

where we note that the magnetization correlation length increases as compared to the noiseless scenario. It is interesting to note that the presence of noise in the anisotropy decreases the magnetization density due to increased defect production, the correlation length of the magnetization correlator, however, increases with the strength of the noise. The amplitude of the magnetization correlator nevertheless decreases with the noise.

B. Spin correlators: $\langle\sigma_x^{1,2}\,\sigma_{x+2n}^{1,2}\rangle$

As shown in Eq. (31) the spin correlators can be expressed as a product of sublattice correlators. One can represent the sublattice correlators at n separation in terms of the determinants of the Toeplitz matrices:

$$\left\langle\left\langle\sigma_x^1\,\sigma_{x+n}^1\right\rangle\right\rangle = D_n[g^{+1,z}], \tag{40}$$

$$\left\langle\left\langle\sigma_x^2\,\sigma_{x+n}^2\right\rangle\right\rangle = D_n[g^{-1,z}], \tag{41}$$

$$\langle\langle\tau_x\,\tau_{x+n}\rangle\rangle = D_n[g^{0,z}], \tag{42}$$

where $g^{m,z}$ are the generating functions defined as

$$g^{m,z}(\xi) = -(-\xi)^m\,(1 - 2\,p_k), \tag{43}$$

where $\xi = e^{2ik}$ and $D_n[g^{m,z}]$ are the corresponding Toeplitz matrix determinants for different sublattice spin correlators. Given the generating function $g^{m,z}$ the determinant $D_n[g^{m,z}]$

are defined as [28,41]

$$D_n[g^{m,z}] = \begin{vmatrix} f_0^{(m)} & f_{-1}^{(m)} & .... & f_{-(n-1)}^{(m)} \\ f_1^{(m)} & f_0^{(m)} & .... & f_{-(n-2)}^{(m)} \\ . & . & .... & . \\ . & . & .... & . \\ . & . & .... & . \\ f_{n-1}^{(m)} & f_{n-2}^{(m)} & .... & f_0^{(m)}, \end{vmatrix}, \tag{44}$$

where the elements of the determinant $f_l^{(m)}$ is the lth cummulant of the generating function $g^{m,z}(\xi) = \sum_l f_l^{(m)} \xi^l$ and are obtained by performing the following contour integration,

$$f_l^{(m)} = \oint_C \frac{d\xi}{2\pi i\xi}\, \xi^{-l}\, g^{m,z}(\xi), \tag{45}$$

where C is a unit circle contour with $|\xi| = 1$. The above integral in terms of the k variable acquires the form

$$f_l^{(m)} = \int_{-\pi/2}^{\pi/2} \frac{dk}{\pi}\, e^{-i2kl}\, g^{m,z}(e^{i2k}). \tag{46}$$

The integral is evaluated by taking the integral representation of the modified Bessel function of the first kind,

$$I_\nu(z) = \frac{1}{2\pi} \int_{-\pi}^{\pi} d\theta e^{z\cos\theta - i\nu\theta}, \tag{47}$$

where ν is an integer and $\mathrm{Re}(z) > 0$. Using the above integral identity yields

$$f_l^{(m)} = \frac{e^{-\pi\bar{z}}}{2\pi}\, I_{l-m}[\pi\bar{z}] - \frac{e^{-\pi(z+\bar{z})}}{\pi}\, I_{l-m}[\pi(z+\bar{z})], \tag{48}$$

with $m = 0, \pm 1$. In the large-z limit (and with $z\eta^2 \neq 0$), the expression reduces to

$$f_l^{(m)} = \frac{(-1)^m}{\pi}\left[\frac{\sqrt{2}\, e^{-(l-m)^2/2\pi(z+\bar{z})}}{\sqrt{z+\bar{z}}} - \frac{e^{-(l-m)^2/2\pi\bar{z}}}{\sqrt{2\bar{z}}}\right].$$

In Figs. 8 and 9 we plot the numerically calculated determinants for the sublattice correlators $\langle\langle \sigma_x^{1,2}\, \sigma_{x+r}^{1,2}\rangle\rangle$ (where r is even separation). Figure 8 corresponds to the noiseless case where we observe the KZ scaling behavior for the correlation length, i.e., larger correlation length for smaller sweep speeds. In Fig. 9 we consider fast noise and use the elements of the Toeplitz matrix given by Eq. (48) to evaluate the determinants. Here we notice the signature of the AKZ behavior, i.e., decrease in the correlation length with the increasing strength of the noise for slower sweeps. Similar behavior is found for the $\langle\langle \tau_x\, \tau_{x+n}\rangle\rangle$ correlator.

C. Spin correlations at large separation

In this section, we investigate the behavior of spin correlators at large separation in the presence of the fast noise. In the asymptotic limit, following Szegö's limit theorem, the Toeplitz determinant acquires the form [28,41,53–56]

$$D_n[g^{m,z}(\xi)] \approx \exp\left[n \int_0^{\pi} \frac{d\theta}{\pi} \ln g^{m,z}(e^{i2\theta})\right], \tag{49}$$

where $g^{m,z}(\xi)$ is the generating function given in Eq. (43).

The zeros of the generating function play an important role in the analyticity of the asymptotic behavior of the spin correlators and it can be easily verified that it has the same set of zeros as the noiseless generating function. Therefore, the effect of zeros of the generating function on the analyticity of the spin correlators with respect to z will remain the same as for the noiseless drive case. The difference is that the generating function with noisy drive is multiplied by an extra noise dependent exponential factor, $e^{-2\pi z \eta_1^2(1-x)}$. We are mainly interested in the role of this extra term on the correlation lengths of the sublattice and the full lattice spin correlators. In the following discussion we will use the method developed by Cherng and Levitov (Ref. [41]) to show that this extra term is responsible for the AKZ scaling behavior of the correlation lengths.

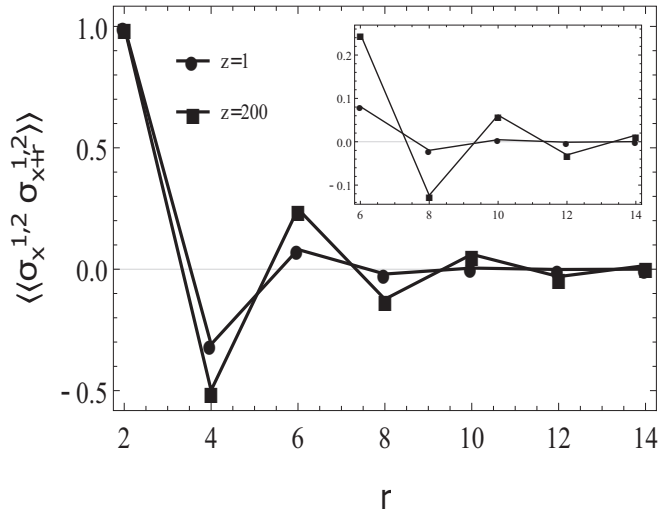

FIG. 8. Sublattice spin correlators $\langle\langle \sigma_x^{1,2}\sigma_{x+r}^{1,2}\rangle\rangle$ have been plotted with respect to the even separation r in the noiseless scenario. The correlators in the figure are normalized from their respective value at separation $r = 2$. From the figure one can observe that the larger z values correspond to the large correlation length which is consistent with the KZ behavior. The correlation length (l_σ) becomes small (short ranged spin correlations) in the fast sweep regime. From the inset one can notice the KZ behavior at relatively larger separation.

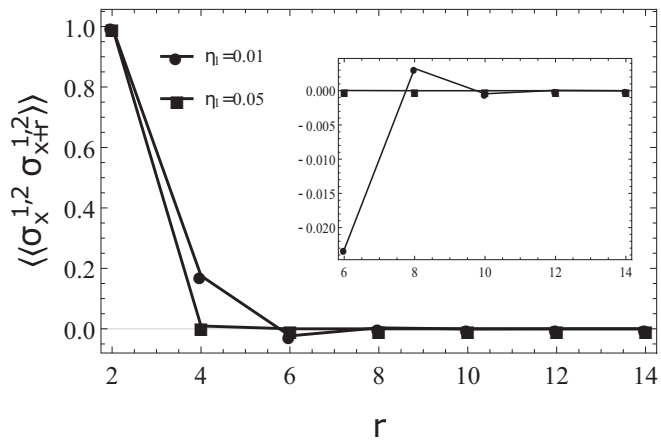

FIG. 9. Normalized $\langle\langle \sigma_x^{1,2}\sigma_{x+r}^{1,2}\rangle\rangle$ vs r for different noise strengths ($\eta_1 = 0.01$ and 0.05) at $z = 200$ (slow sweep regime). The correlation length l_σ decreases with the increased noise strength, which is the signature of AKZ scaling behavior.

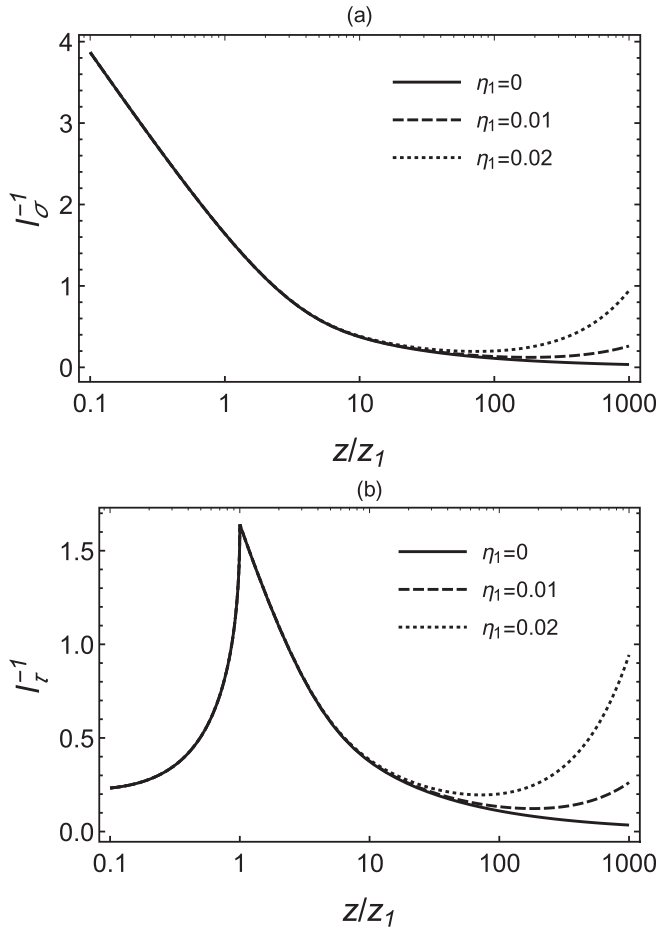

FIG. 10. The sublattice inverse correlation lengths have been plotted as a function of z for the different noise strengths; both the l_σ^{-1} and l_τ^{-1} show the anti-Kibble-Zurek scaling behavior, i.e., the inverse sublattice correlation lengths $l_{\sigma,\tau}$ increases after an optimal quench parameter ($\sim z_{\rm O}$) which depends on the noise strength. In contrast, for the noiseless case both l_σ^{-1} and l_τ^{-1} exhibit monotonic suppression for large z regime. Furthermore, the l_τ^{-1} shows nonanalytical behavior at $z = z_1$ and beyond $z > z_1$ both have the same values. Therefore, it is understood that the increased noise strength of the fast noise further decreases l, making the spin correlators relatively short ranged in the presence of the fast noise. The $l^{-1} = l_\sigma^{-1} + l_\tau^{-1}$ also shows the nonanalytical behavior at $z = z_1$ as a result of the nonanalytical behavior of l_τ^{-1}; this is the indication of the crossover of different behaviors of the spin correlators, i.e., nonoscillatory monotonically decreasing behavior for $z < z_1$ regime and exponentially suppressed oscillatory behavior of spin correlators for $z > z_1$ regime with respect to the spatial separation.

The generating function for the noisy drive can be written as

$$g_{\rm fn}^{m,z}(\xi) = -(-\xi)^m \lambda_0^{-1}(1-\lambda_0\xi)(1-\lambda_0\xi^{-1})\, e^{H(\xi)}, \quad (50)$$

where

$$H(\xi) = h(\xi) - 2\pi\, z\, \eta_1^2(1-x), \quad (51)$$

and

$$h(\xi) = \ln\left[\frac{1-e^{-\pi\, z(1-2\,z_1/z-x)}}{2(1-2\,z_1/z-x)}\right]. \quad (52)$$

The zeros closest to the unit circle are denoted by λ_0 and λ_0^{-1}, where $\lambda_0 = 1/\exp[\cosh^{-1}(1-2z_1/z)]$. Both $h(\xi)$ and $H(\xi)$ can be expanded as a function of $x = (\xi + \xi^{-1})/2$ as follows,

$$h(x) = \sum_{n\geqslant 0} h_n\, x^n, \quad H(x) = \sum_{n\geqslant 0} H_n\, x^n, \quad (53)$$

where we notice that $H_0 = h_0 - 2\pi\, z\, \eta_1^2$ and $H_1 = h_1 + 2\pi\, z\, \eta_1^2$, while for $n \neq 0, 1$, all other coefficients satisfy $H_n = h_n$. The correlation length of the sublattice spin correlators are given by the following expression

$$l_{\sigma/\tau}^{-1} = -\int_{-1}^{1} \frac{dx}{\sqrt{1-x^2}}\, H(x) = -\int_{-1}^{1} \frac{dx}{\sqrt{1-x^2}}\, h(x) + \pi^2 \bar{z}, \quad (54)$$

where the full lattice correlator is given by $l^{-1} = l_\sigma^{-1} + l_\tau^{-1}$. The result of the above integration yields

$$l_{\sigma/\tau}^{-1} \approx \sum_{m=0}^{\infty} \frac{\Gamma(m+1/2)^2\, {\rm Re}\, Li_{m+3/2}(2)}{\pi^{3/2}\,\Gamma(m+1)(2\pi\, z)^{m+1/2}} + \pi^2 \bar{z}, \quad (55)$$

where the summation term is due to the noiseless case [41], which in the limit of slow sweep speed results in the correlation length or the domain size proportional to $\sqrt{z}$ (from the dominant $m = 0$ term) thus satisfying the KZ scenario. On the other hand, the presence of the additional $\pi^2\bar{z}$ term due to the fast noise in the large z scenario results in the scaling of the correlation length to be consistent with the AKZ picture suggesting that the domain size reduces. This result quantifies how the fast noise randomizes the driven system spatially at the end of the protocol. The sublattice correlation lengths have been plotted in Fig. 10 with respect to z for different noise strengths. They clearly show the AKZ behavior in the large-z case, i.e., beyond quench parameters of the order of $z_{\rm O}$ the inverse correlation length starts to increase. For small-z values the fast noise has negligible effect.

VII. CONCLUDING REMARKS

In this work we quantify analytically the effects of the fast Gaussian noise in the driven quantum XY-spin chain. We have considered transverse protocol in which the external transverse magnetic field drives the system linearly with respect to time, starting from the paramagnetic phase to a region with the ferromagnetic phase and finally back to the paramagnetic phase in the presence of the time dependent Gaussian noise in the anisotropy term. In this protocol, the system passes through two quantum critical points at $h = \mp J$ where the energy gap vanishes resulting in nonadiabatic effects. We map the problem to the noisy LZ problem, and in terms of the density matrix formalism we obtain a reduced master equation for the population inversion. The solution of the equation in the $T \to \infty$ limit has been utilized to obtain the final excitation probability. We show that the defect density exhibits AKZ scaling behavior in the slow sweep regime, and the optimal quench time which minimizes the defect density is shown to scale as $\eta_0^{-4/3}$ with the noise strength.

The implications for the correlators due to the nonequilibrium dynamics of the noisy transverse drive protocol are as follows: First, the fast fluctuating coherences vanishes in the

large time limit (even without the noise) due to the internal decoherence arising from the large system size ($N \to \infty$) and this allows the course graining in momentum space and transforms the pure state into an entropic state with finite nonzero entropy. The time dependent Gaussian fast noise further exponentially suppresses the highly fluctuating coherences and in particular affects the system most when the system passes through the quantum critical points. Finally, the noise can heat up the population to the asymptotic infinite temperature state for the slower sweeps or large-z case, maximizing the entropy density to $\log 2$ and at the same time minimizing the average magnetization density to zero. The effects of the noise are minimized when driven at an optimal sweep rate which turns out to scale universally with the strength of the fast noise.

We have analyzed the spin-spin correlation functions (in the presence of noise) at the end of the protocol for large separation using the Toeplitz determinant asymptotes at large n. For slow sweep speeds the effect of the fast Gaussian noise on the correlation lengths of the spin correlators at large separation reveals behavior consistent with the anti-Kibble-Zurek picture. The sublattice correlation lengths for $\sigma^{1,2}$ and τ-spin correlators decreases with the strength of the noise according to the anti-Kibble-Zurek scaling behavior. We have also analyzed the effect of the fast noise on the magnetization σ^3-spin correlator. For large n separation we find that the correlation length of the magnetization correlator increases with the strength of noise when $\eta_1 \ll 1$ and $\pi\bar{z} < 1$.

ACKNOWLEDGMENT

S.G. is grateful to the SERB, Government of India, for the support via the Core Research Grant No. CRG/2020/002731.

[1] T. W. B. Kibble, J. Phys. A: Math. Gen. **9**, 1387 (1976).
[2] T. Kibble, Phys. Rep. **67**, 183 (1980).
[3] W. H. Zurek, Nature (London) **317**, 505 (1985).
[4] T. W. B. Kibble, Nature (London) **317**, 472 (1985).
[5] W. H. Zurek, Nature (London) **368**, 292 (1994).
[6] W. Zurek, Phys. Rep. **276**, 177 (1996).
[7] A. del Campo and W. H. Zurek, Int. J. Mod. Phys. A **29**, 1430018 (2014).
[8] B. Damski, Phys. Rev. Lett. **95**, 035701 (2005).
[9] W. H. Zurek, U. Dorner, and P. Zoller, Phys. Rev. Lett. **95**, 105701 (2005).
[10] J. Dziarmaga, Phys. Rev. Lett. **95**, 245701 (2005).
[11] A. Polkovnikov, Phys. Rev. B **72**, 161201(R) (2005).
[12] A. Polkovnikov, K. Sengupta, A. Silva, and M. Vengalattore, Rev. Mod. Phys. **83**, 863 (2011).
[13] G. Lamporesi, S. Donadello, S. Serafini, F. Dalfovo, and G. Ferrari, Nat. Phys. **9**, 656 (2013).
[14] J.-M. Cui, Y.-F. Huang, Z. Wang, D.-Y. Cao, J. Wang, W.-M. Lv, L. Luo, A. del Campo, Y.-J. Han, C.-F. Li, and G.-C. Guo, Sci. Rep. **6**, 33381 (2016).
[15] A. Keesling, A. Omran, H. Levine, H. Bernien, H. Pichler, S. Choi, R. Samajdar, S. Schwartz, P. Silvi, S. Sachdev, P. Zoller, M. Endres, M. Greiner, V. Vuletić, and M. D. Lukin, Nature (London) **568**, 207 (2019).
[16] J. Dziarmaga, Phys. Rev. B **74**, 064416 (2006).
[17] S. Mostame, G. Schaller, and R. Schützhold, Phys. Rev. A **76**, 030304(R) (2007).
[18] A. Fubini, G. Falci, and A. Osterloh, New J. Phys. **9**, 134 (2007).
[19] D. Patanè, A. Silva, L. Amico, R. Fazio, and G. E. Santoro, Phys. Rev. Lett. **101**, 175701 (2008).
[20] D. Patanè, L. Amico, A. Silva, R. Fazio, and G. E. Santoro, Phys. Rev. B **80**, 024302 (2009).
[21] A. Niederberger, M. M. Rams, J. Dziarmaga, F. M. Cucchietti, J. Wehr, and M. Lewenstein, Phys. Rev. A **82**, 013630 (2010).
[22] T. Prosen, Phys. Rev. Lett. **107**, 137201 (2011).
[23] T. Prosen, Phys. Rev. Lett. **106**, 217206 (2011).
[24] D. Poletti, J.-S. Bernier, A. Georges, and C. Kollath, Phys. Rev. Lett. **109**, 045302 (2012).
[25] J. Marino and A. Silva, Phys. Rev. B **86**, 060408(R) (2012).
[26] Z. Cai and T. Barthel, Phys. Rev. Lett. **111**, 150403 (2013).
[27] L. D'Alessio and A. Rahmani, Phys. Rev. B **87**, 174301 (2013).
[28] J. Marino and A. Silva, Phys. Rev. B **89**, 024303 (2014).
[29] U. Marzolino and T. Prosen, Phys. Rev. A **90**, 062130 (2014).
[30] D. Zueco, P. Hänggi, and S. Kohler, New J. Phys. **10**, 115012 (2008).
[31] K. Shimizu, Y. Kuno, T. Hirano, and I. Ichinose, Phys. Rev. A **97**, 033626 (2018).
[32] S. Bandyopadhyay, S. Bhattacharjee, and A. Dutta, Phys. Rev. B **101**, 104307 (2020).
[33] P. Weinberg, M. Tylutki, J. M. Rönkkö, J. Westerholm, J. A. Åström, P. Manninen, P. Törmä, and A. W. Sandvik, Phys. Rev. Lett. **124**, 090502 (2020).
[34] S. M. Griffin, M. Lilienblum, K. T. Delaney, Y. Kumagai, M. Fiebig, and N. A. Spaldin, Phys. Rev. X **2**, 041022 (2012).
[35] V. Yukalov, A. Novikov, and V. Bagnato, Phys. Lett. A **379**, 1366 (2015).
[36] A. Dutta, A. Rahmani, and A. del Campo, Phys. Rev. Lett. **117**, 080402 (2016).
[37] Z.-P. Gao, D.-W. Zhang, Y. Yu, and S.-L. Zhu, Phys. Rev. B **95**, 224303 (2017).
[38] Q. N. Meier, M. Lilienblum, S. M. Griffin, K. Conder, E. Pomjakushina, Z. Yan, E. Bourret, D. Meier, F. Lichtenberg, E. K. H. Salje, N. A. Spaldin, M. Fiebig, and A. Cano, Phys. Rev. X **7**, 041014 (2017).
[39] B. Gardas, J. Dziarmaga, W. H. Zurek, and M. Zwolak, Sci. Rep. **8**, 4539 (2018).
[40] R. Puebla, A. Smirne, S. F. Huelga, and M. B. Plenio, Phys. Rev. Lett. **124**, 230602 (2020).
[41] R. W. Cherng and L. S. Levitov, Phys. Rev. A **73**, 043614 (2006).
[42] L. Cincio, J. Dziarmaga, M. M. Rams, and W. H. Zurek, Phys. Rev. A **75**, 052321 (2007).
[43] K. Sengupta, D. Sen, and S. Mondal, Phys. Rev. Lett. **100**, 077204 (2008).
[44] S. Mondal, D. Sen, and K. Sengupta, Phys. Rev. B **78**, 045101 (2008).
[45] S. Mondal, K. Sengupta, and D. Sen, Phys. Rev. B **79**, 045128 (2009).

[46] U. Divakaran, V. Mukherjee, A. Dutta, and D. Sen, J. Stat. Mech.: Theory Exp. (2009) P02007.

[47] U. Divakaran, A. Dutta, and D. Sen, Phys. Rev. B **78**, 144301 (2008).

[48] A. Dutta, G. Aeppli, B. K. Chakrabarti, U. Divakaran, T. F. Rosenbaum, and D. Sen, *Quantum Phase Transitions in Transverse Field Spin Models: From Statistical Physics to Quantum Information* (Cambridge University Press, New Delhi, 2015).

[49] V. L. Pokrovsky and N. A. Sinitsyn, Phys. Rev. B **67**, 144303 (2003).

[50] M. B. Kenmoe, H. N. Phien, M. N. Kiselev, and L. C. Fai, Phys. Rev. B **87**, 224301 (2013).

[51] R. K. Malla, E. G. Mishchenko, and M. E. Raikh, Phys. Rev. B **96**, 075419 (2017).

[52] M.-Z. Ai, J.-M. Cui, R. He, Z.-H. Qian, X.-X. Gao, Y.-F. Huang, C.-F. Li, and G.-C. Guo, Phys. Rev. A **103**, 012608 (2021).

[53] E. Lieb, T. Schultz, and D. Mattis, Ann. Phys. **16**, 407 (1961).

[54] E. Barouch and B. M. McCoy, Phys. Rev. A **3**, 786 (1971).

[55] E. L. Basor and K. E. Morrison, Linear Algebra and its Applications **202**, 129 (1994).

[56] P. J. Forrester and N. E. Frankel, J. Math. Phys. **45**, 2003 (2004).